Coarsening of fine-scale exsolution lamellae

John B. Brady

Geology Department, Smith College, Northampton, Massachusetts 01063, U.S.A.

Abstract

Diffusional exchange between the wedge-shaped terminations of fine-scale, coherent exsolution lamellae and the large flat sides of adjacent like lamellae is proposed as the principal mechanism for the coarsening of lamellar exsolution textures in silicate minerals. Following the methods of Gibbs (1906), a formula is derived for the chemical potential gradients due to interfacial energy effects that drive the proposed diffusion and coarsening. The calculated driving force is shown to be inversely proportional to the lamellar wavelength (λ), as obtained by Cline (1971) for a similar geometry. For this model of lamellar coarsening, the appropriate rate law is given by $\lambda^2 = \lambda_0^2 + kt$ rather than the rate law ($\lambda = \lambda_0 + kt^{1/3}$) that applies to the coarsening of more equidimensional precipitates (Wagner, 1961). For geologic problems, extrapolation of the data of laboratory coarsening experiments using the λ^2 rate law yields results significantly different from those obtained using the $t^{1/3}$ rate law, if the coarsening event lasts more than a few hundred years. The rate of coarsening, according to the proposed model, depends on the two-dimensional density of wedge-shaped ends (WSE), i.e., their number per unit cross-sectional area (n_{WSE}). Measurements of TEM photos of clinopyroxenes, exsolved and coarsened at 1000°C by Nord and McCallister (1979), give WSE densities in the range 1×10^{12} to 15×10^{12} m^{-2}. The product λn_{WSE} should be constant during coarsening and has been determined to be in the range 1×10^5 to 5×10^5 m^{-1} for the same exsolved clinopyroxenes.

Introduction

Exsolution textures in synthetic minerals have been observed to coarsen when annealed at appropriate temperatures in the laboratory (Yund et al., 1974; Park et al., 1976; Yund and Davidson, 1978; McCallister, 1978; Nord, 1980; Grove, 1982). Although it is commonly believed that the mechanism for this coarsening is related to "imperfections" in the microstructure (Graham and Kraft, 1966; Cline, 1971; Lin and Courtney, 1974; Courtney, 1975), the microscopic details of the coarsening process are not fully understood. Because geologic applications of coarsening studies typically require long extrapolations of the results of short experiments, it is important that the theoretical basis for these extrapolations be firm. This paper explores the consequences of certain assumptions about the coarsening of lamellar intergrowths of minerals formed by exsolution. It will be demonstrated that the rate law currently in use to describe the kinetics of coarsening of lamellar textures is incorrect and may lead to significant errors if used to apply laboratory data to natural processes lasting thousands of years.

Coarsening of exsolution lamellae is an example of a set of processes that have been called "Ostwald ripening" after the experiments of W. Ostwald (1900). Ostwald observed that the solubility of various crystals in aqueous solutions was greater for small crystals than for large crystals. Indeed, he was able to demonstrate that small crys-

tals would dissolve in a solution from which large crystals of the same compound would grow. The difference in solubility can be attributed to the higher specific free energy of small crystals relative to large crystals, owing to the greater surface-to-volume ratio of the small crystals. Similarly, when exsolution lamellae coarsen, some lamellae must grow and others must be eliminated such that the average surface-to-volume ratio of the lamellae is decreased.

The driving force for the coarsening process is a reduction of free energy due to the reduction of surface or interfacial area. The reduction of surface area that accompanies the dissolution of one crystal and the growth of a nearby crystal is clear in Ostwald's experiments. So too are the chemical potential gradients that drive diffusion from a small crystal of higher specific free energy to a nearby large crystal of lower specific free energy. The reduction of interfacial area that accompanies the coarsening of exsolution lamellae also seems clear enough until the microscopic details of the process are examined.

Imagine a set of perfectly tabular exsolution lamellae like those shown in Figure 1a. Assume for the purposes of discussion that the shaded lamellae coarsen "actively" by diffusive exchange of material and that the unshaded lamellae coarsen "passively" by the elimination of shaded lamellae. At an intermediate stage in this hypothetical coarsening process, the lamellae might look like Figure 1b, where the lamellae have alternately increased and de-
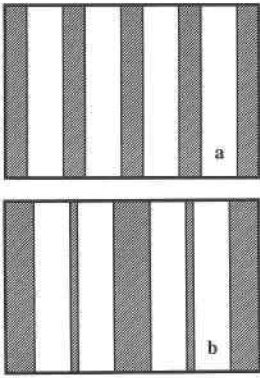
Fig. 1. Hypothetical coarsening of perfect lamellae (a) through an intermediate stage (b). Because surface area is not eliminated until the entire lamella is consumed, perfect lamellae will not coarsen.

creased in width at constant total volume. Although it appears that coarsening is proceeding nicely as the lamellae change from the configuration of Figure 1a to that of Figure 1b, in fact there has been *no reduction of interfacial area*. Perfect lamellae cannot coarsen in any continuous process because there is no reduction in free energy to drive the coarsening through the intermediate stages. Discontinuous coarsening in which a grain boundary moves through the exsolved crystal (Livingston and Cahn, 1974; Fournelle, 1979a, 1979b) may be possible for perfect lamellae, but this does not explain the observed (e.g., Yund and Davidson, 1978; McCallister, 1978) continuous coarsening of exsolved synthetic minerals in the laboratory.

A COARSENING MODEL

Exsolution lamellae observed in minerals are not perfect; they typically branch and terminate in a variety of ways. Examples may be found in Figure 2, TEM images of exsolved synthetic pyroxenes. Textures like these are considered to be typical of minerals exsolved through the process of spinodal decomposition (Yund, 1984), but they do not prove that the exsolution mechanism was spinodal decomposition rather than nucleation and growth. Although three-dimensional information is averaged to produce the two-dimensional TEM photo, it appears that the lamellar "terminations" or "faults" are wedge shaped with little curvature in the third dimension—at least within the 0.5-μm thickness of the TEM section. It is the thesis of this paper that coarsening of exsolution lamellae may occur by the diffusion of material from these wedge-shaped ends across adjacent unlike lamellae to be added to similar lamellae nearby (see Fig. 3). As material is lost from a wedge-shaped end (WSE), its position changes, allowing the adjacent (unshaded) lamellae to become continuous. Geometrically, this process is reminiscent of the action of a zipper. Because the lamella that has a WSE is being continuously consumed as the "zipper" closes, interfacial area and its associated free energy are continuously decreasing. This is not a new model; it has been
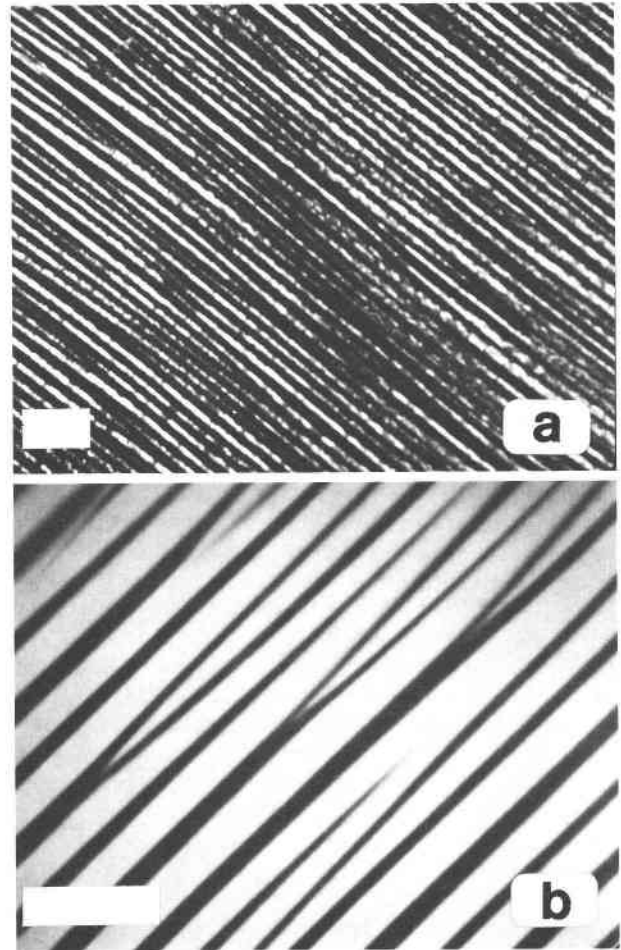

Fig. 2. Dark-field transmission-electron-microscope images of exsolved clinopyroxenes from the study of Nord and McCallister (1979). See also Buseck et al. (1980, Fig. 23). If the figures are viewed parallel to the lamellae, the wedge-shaped ends are more apparent. The bright phase is pigeonite and the dark phase is augite. The sample in (a) was annealed for 1075 h at 1000°C; the sample in (b) was annealed for 3838 h at 1000°C. The white scale represents 0.2 μm. Photographs taken by Gordon Nord.

extensively developed in the materials-science literature (Graham and Kraft, 1966; Cline, 1971). Annealing experiments of lamellar metal intergrowths have verified the movement of lamellar terminations (Lin and Courtney, 1974; Garmong and Rhodes, 1974). Nevertheless, coherent exsolution lamellae in minerals are sufficiently different from metal intergrowths to warrant a detailed analysis.

Coarsening of exsolution lamellae in silicate minerals requires diffusion of only a few cations within a fixed framework of oxygen atoms. For example, coarsening in cryptoperthite is accomplished by the diffusion of K and Na; no diffusion of oxygen (or Al and Si) is needed. Diffusion is driven by chemical potential gradients, which are generally reflected by gradients in chemical compo-

sition. If the proposed model of lamellar coarsening is correct, chemical potential gradients must exist between each WSE and the thickened lamellae nearby. Two reasons immediately come to mind why chemical potential gradients should exist. (1) The chemical potential of a component defined by local equilibrium with the WSE of a lamella should exceed the chemical potential of that component defined by local equilibrium with the adjacent like lamella, because of the higher interfacial free energy of the WSE facets. (2) A concentration of strain energy in the vicinity of the WSE is expected over and above the homogeneous strain energy that accompanies coherent exsolution (Robin, 1974a, 1974b).

The shape of the WSE's is typically much "sharper" than would be expected for the equilibrium form of a strain-free faceted crystal (see Johnson, 1965), suggesting that factors in addition to interfacial energy combine to determine the WSE shape. Sharp WSEs may reflect the influence of the strain-energy concentration expected near lamellar terminations in coherent crystals. However, even though strain energy may affect the shape of WSEs, strain energy probably does not contribute significantly to the driving force for coarsening. For lamellae with no curvature in the third dimension, migration of a WSE changes the *location* of the extra strain energy, but the strain energy is not *eliminated* as long as the WSE exists. Using the strain-energy concentration at the WSE to drive the diffusion that leads to WSE migration would violate the second law of thermodynamics: getting diffusion work without the expenditure of energy. Interfacial area *is* eliminated as the WSE retreats, making interfacial free energy an acceptable driving force. Oriani (1964), using a slightly different argument, has similarly concluded that coarsening of coherent precipitates is driven by interfacial free energy, not strain effects. If the lamellae are actually disc-shaped in plan (WSEs curved perpendicular to the plane of Fig. 3), then WSE migration would lead to a shrinking lamellar disc and a consequent reduction in strain energy. In this case, strain energy could contribute to the driving force for coarsening. Because the magnitude of this curvature is unknown, the following analysis will proceed on the assumption that interfacial energy is the driving force for coarsening.

SOME THERMODYNAMICS

To examine the quantitative implications of this model for geologic applications, it is necessary to develop a mathematical formalism. In this endeavor I will follow very closely the analysis of Cline (1971), who considered the coarsening and stability of directionally solidified lamellar eutectics as an addendum to a detailed discussion of rod-shaped composite structures. The model assumes that diffusion is the rate-limiting process for coarsening. Therefore, the first step in the analysis is to obtain an expression for the chemical potential gradients and related concentration gradients that drive diffusion from a WSE to adjacent like lamellae. Because the WSEs of mineral lamellae are bounded by approximately flat, facetlike
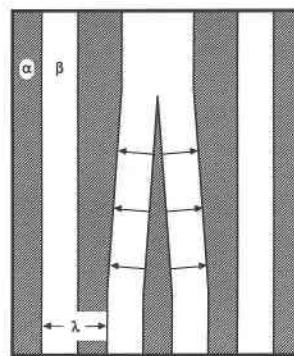

Fig. 3. A cross section of an exsolved mineral of host β and guest α showing an ideal wedge-shaped end (WSE). λ is the lamellar wavelength prior to coarsening. The arrows show schematically the diffusion that will lead to movement of the WSE.

surfaces, it is not possible to follow Cline (1971) directly and use the Gibbs-Thompson equation (Lewis and Randall, 1961, Eq. 29-34) for the chemical potential near spherical interfaces. Similarly, because coherent exsolution lamellae do not have a strain-free equilibrium form, Johnson's (1965, Eq. 13) modified Gibbs-Thompson equation for centrosymmetric crystals in "shape equilibrium" cannot be used. The analysis requires a different equation from Gibbs with a modification for two-component crystals.

Gibbs (1906, Eq. 665), repeated in Herring (1951, Eq. 18), considered the free-energy change that would attend the infinitesimal growth or dissolution of a single facet of a crystal. At equilibrium, this free-energy change must be zero. Gibbs obtained an expression for the chemical potential $\mu_A(i)$ of component A in a fluid adjacent to crystal face i of a crystal of pure A, relative to the chemical potential $\mu_A(\infty)$ of component A defined by an infinitely large crystal of A, as follows:

$$\mu_A(i) - \mu_A(\infty) = (v_A/S_i) \sum_j [\gamma_j \csc(\varphi_{ij}) - \gamma_i \mathrm{ctn}(\varphi_{ij})] \cdot L_{ij}, \quad (1)$$

where v_A is the molar volume of the crystal, S_i is the surface area of facet i, γ_i is the interfacial energy of facet i, γ_j is the interfacial energy of adjacent facet j, φ_{ij} is the dihedral angle between facet i and the extension of facet j, and L_{ij} is the length of the edge between facets i and j. (Symbols are collected in Table 1 for reference.) The summation in Equation 1 is over all facets j adjacent to facet i. Gibbs (1906) pointed out that if the crystal is to have an equilibrium form, the summation in Equation 1 divided by the surface area S_i must be the same for all facets. Conversely, if the crystal does not have an equilibrium form, the summation in Equation 1 divided by the surface area S_i will not be the same for all facets, and $\mu_A(i)$ will vary in the matrix around the crystal. Because in this case the chemical potential determined by Equation 1 would not be single-valued at the intersection of two facets, it is likely that the crystal edges are rounded

TABLE 1. List of symbols and units

$\Delta C_{A\beta}$	the difference between the concentration of component A in the matrix phase β near a WSE of a lamella of phase α and the concentration of component A in the matrix phase β near the LFS of an adjacent α lamella (moles of A per cubic meter)
D_{AB}	the A $\rightleftharpoons$ B interdiffusion coefficient in phase β (m²/s)
dH	infinitesimal length lost from an exsolution lamella during coarsening as shown in Figure 4b (m)
J_A	diffusional flux (per unit length of WSE) of component A (in moles) from one facet of a WSE (moles of A per meter of WSE per second)
k	a constant given by Equation 21 (m²/s)
K_1	a constant given by Equation 7 (moles of A per square meter)
K_2	a constant given by Equation 8 (dimensionless)
K_3	a constant given by Equation 13 (m³/s)
L_{ij}	length of the edge in common between adjacent facets i and j (m)
L_S	length of the short edge of one WSE facet (m)
L_{WSE}	length of the long edge of one WSE facet (m)
LFS	the large flat side of an exsolution lamella
n_{WSE}	the two-dimensional density of WSEs, i.e., the average number of WSEs per unit cross-sectional area (m⁻²)
$n_{WSE,0}$	n_{WSE} at the start of coarsening (m⁻²)
R	ideal-gas constant (8.314 J·mol⁻¹ K⁻¹)
S_i	surface area of facet i of a crystal (m²)
S_{WSE}	surface area of one facet of a WSE per unit length of WSE (m)
T	absolute temperature (K)
v_A	molar volume of a crystal of pure A (m³/mol)
v_α	molar volume of a crystal of phase α (m³/mol)
V^e_{WSE}	average velocity of the WSEs of lamellae of phase α as they recede during coarsening (m/s)
$X_{A\alpha}(WSE)$	mole fraction of component A in phase α at the WSE of an exsolution lamella of α (dimensionless)
$X_{A\beta}(\infty)$	mole fraction of component A in exsolved phase β for a coarse (∞), no interfacial energy effect (coherent), equilibrium composition (dimensionless)
X_B	bulk composition of the mineral grain (host + exsolved guest) containing α and β given as the mole fraction of component B
dZ	cross-sectional area of infinitesimal volume lost from one facet of a WSE, defined in Figure 4b
γ_i	interfacial free energy of facet i of a crystal (J/m²)
γ_{LFS}	interfacial free energy of the large flat side of an exsolution lamella (J/m²)
φ	dihedral angle between a WSE facet and the extension of the LFS of an exsolution lamella (see Fig. 4b)
φ_{ij}	dihedral angle between facet i and the extension of facet j
λ	lamellar wavelength (m)
λ_α	thickness of lamellae of phase α (m)
λ_0	lamellar wavelength at the start of coarsening (m)
$\mu_A(i)$	chemical potential of component A in a fluid adjacent to crystal face i of a crystal of pure A (joules per mole of A)
$\mu_A(\infty)$	chemical potential of component A defined by an infinitely large crystal of A (joules per mole of A)
$\mu_{A\beta}(\infty)$	chemical potential of component A in phase β in equilibrium with a crystal of infinite size of phase α (joules per mole of A)
$\mu_{A\beta}(WSE)$	chemical potential of component A in phase β in equilibrium with a WSE of a lamella of phase α (joules per mole of A)
$\Delta\mu_{A\beta}$	difference in the chemical potential of component A in phase β between a WSE and the LFS of an adjacent like lamella

on some scale. Gibbs did not explicitly discuss crystals like the exsolution lamellae considered here where kinetic factors preserve crystals that do not have a strain-free equilibrium form. Nevertheless, his derivation appears to apply to this specialized case of local equilibrium. Gibbs derived Equation 1 for a crystal in equilibrium with a liquid, but there is nothing in the nature of the derivation that precludes its application to a small crystal included in a larger crystal.

Some simplification of Equation 1 is possible for WSEs, because of the symmetry of the WSEs and the shape of the lamellae. Ideally, each of the two facets on a WSE has four edges (E1 to E4 in Fig. 4a), and the summation in Equation 1 would be to $j = 4$. However, because of the planar geometry of the lamellae, the L_j terms for two of the WSE edges (E1 and E3) are very small relative to the other two L_j terms ($L_{WSE} \gg L_S$), so that two of the four edges in the summation can be neglected. If reflection symmetry of the WSE (see Fig. 4b) is maintained, both facets of the WSE grow or recede simultaneously, the surface area S_{WSE} of each facet is constant, the cotangent terms are eliminated in the summation, and Equation 1 becomes

$$\mu_{A\beta}(WSE) - \mu_{A\beta}(\infty) = v_A(L_{WSE}/S_{WSE})[\gamma_{LFS}\csc(\varphi)], \quad (2)$$

where $\mu_{A\beta}(WSE)$ is the chemical potential of component A in phase β in equilibrium with a WSE of α, L_{WSE} is the long edge of the WSE facet, the subscript LFS refers to the large flat side of a lamella, and the angle φ is as shown in Figure 4b. Now $S_{WSE} = L_{WSE}L_S$ and $L_S = \lambda_\alpha/[2\sin(\varphi)]$ (see Fig. 4). Substituting these relations and using the identity $1/\sin(\varphi) = \csc(\varphi)$, Equation 2 becomes

$$\mu_{A\beta}(WSE) - \mu_{A\beta}(\infty) = 2v_A\gamma_{LFS}/\lambda_\alpha, \quad (3)$$

where λ_α is the average width of the WSE lamellae. Note that it is γ_{LFS} that appears in Equation 3, not γ_{WSE}. This makes sense because it is the sides of the lamellae that are eliminated during coarsening. Garmong and Rhodes (1974, p. 2513) reached the same conclusion using a more qualitative argument. Because the LFSs of the exsolution lamellae have surface areas that are much larger than the areas of the WSE facets, the value of $\mu_{A\beta}(LFS) - \mu_{A\beta}(\infty)$ is many times smaller than the value of $\mu_{A\beta}(WSE) - \mu_{A\beta}(\infty)$. Thus, Equation 3 gives the difference in the chemical potential ($\Delta\mu_{A\beta}$) of component A in phase β between the WSE of a lamella of pure A and the LFS of an adjacent lamella of pure A.

In all of the preceding analysis, the crystal or lamella was assumed to be a one-component phase while the surrounding fluid or matrix was of variable composition. For real exsolution lamellae, two or more components must be considered for both phases. Taking the case that both the WSE phase α and the matrix phase β are solid solutions of the two components A and B and neglecting the variations in the molar volumes of α and β over the composition ranges considered, Equation 3 is modified (following the procedures of Gibbs, 1906, p. 316–321) to read

$$\begin{aligned} \mu_{A\beta}(WSE)X_{A\alpha}(WSE) &+ \mu_{B\beta}(WSE)X_{B\alpha}(WSE) \\ - \mu_{A\beta}(\infty)X_{A\alpha}(\infty) &- \mu_{B\beta}(\infty)X_{B\alpha}(\infty) \\ &= 2v_\alpha\gamma_{LFS}/\lambda_\alpha. \end{aligned} \quad (4)$$

In this expression, $X_{A\alpha}(WSE)$ is the mole fraction of component A in phase α at the WSE, $X_{B\alpha}(\infty)$ is the mole fraction of component B in an infinitely large crystal of phase α, etc. Rearrangement of Equation 4 to a more

usable form is accomplished in Appendix 1 with the help of the following assumptions: (1) that there is no appreciable compositional variation within a lamella near its WSE, (2) that the activity coefficient for component A does not vary significantly with position in either phase α or in phase β, both of which have virtually uniform compositions, and (3) that the molar volumes of α and β do not vary dramatically with composition. The result (Eq. A9) is as follows:

$$\Delta C_{A\beta} = K_1/\lambda, \qquad (5)$$

where $\Delta C_{A\beta}$ is the difference between the concentration of component A in the matrix phase β near a WSE and the concentration of component A in the matrix phase β near the LFS of an adjacent lamella. K_1 is a constant given by

$$K_1 = [2v_\alpha\gamma_{LFS}X_{A\beta}X_{B\beta}]/[K_2RTv_\beta(X_{B\beta} - X_{B\alpha})] \qquad (6)$$

in which R is the gas constant, T is the absolute temperature, and all of the mole fractions are for the coarse (∞), equilibrium compositions. K_2 is also a constant given by

$$K_2 = \lambda_\alpha/\lambda = 1 - \lambda_\beta/\lambda = (X_{B\beta} - X_B)v_\alpha/[(X_{B\beta} - X_B)v_\alpha \\ + (X_B - X_{B\alpha})v_\beta] \qquad (7)$$

in which λ_α is the average width of the WSE lamellae, λ is the lamellar wavelength, X_B is the bulk composition of the exsolved mineral containing α and β given as the mole fraction of component B. What follows depends on the form of Equation 5, but not on the value of the constant K_1.

The basic statement of Equation 5 is that the driving force for the diffusion that leads to WSE migration and lamellar coarsening is proportional to $1/\lambda$. This is the same result that Cline (1971) presented for lamellae with hemicylindrical ends. It is reasonable and intuitively satisfying that the result should not depend on whether the lamellar ends are round or faceted. Proportionality of the driving force to $1/\lambda$ is probably also correct for other WSE geometries.

KINETICS

Using Equation 5 it is possible to discover the migration velocity V_{WSE} of an average WSE. WSE migration occurs as material diffuses from the WSE to the adjacent like lamellae. This diffusion is steady-state in a reference frame that moves with the WSE because the chemical potential gradient $\Delta\mu_{A\beta}$ and the diffusion distance λ_β do not change as the WSE moves (see Fig. 4b). Using Fick's law and assuming that the diffusion is one-dimensional in a two-component system, the steady-state flux J_A (*per unit length* of WSE) from one facet of a WSE is given by

$$J_A = S_{WSE}D_{AB}[\Delta C_{A\beta}/\lambda_\beta], \qquad (8)$$

where S_{WSE} is the surface area of one facet of a WSE *per unit length* of WSE, D_{AB} is the A $\rightleftharpoons$ B interdiffusion coefficient, and $\Delta C_{A\beta}$ is the concentration difference between the WSE and the adjacent like lamellae. Equation 5 for
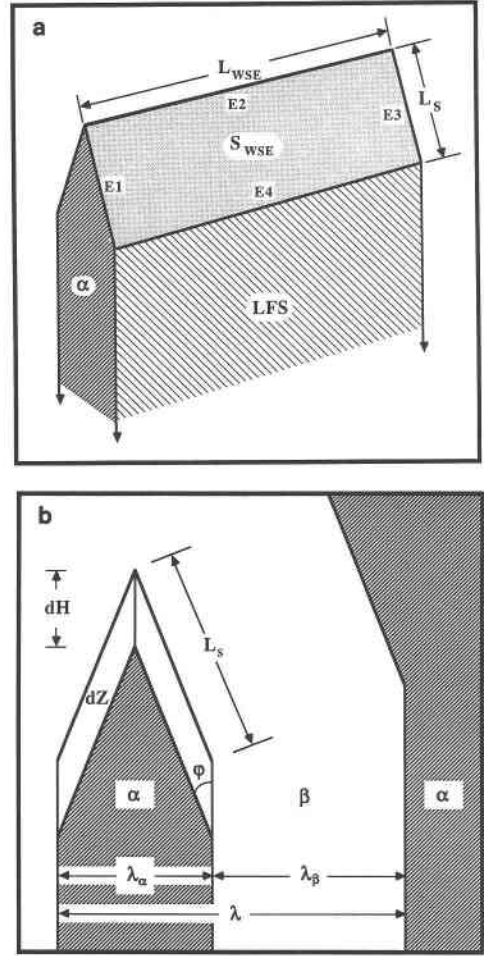

Fig. 4. A distorted and enlarged wedge-shaped end (WSE) of a lamella of phase α drawn to clarify parameters used in the text: (a) foreshortened perspective view, (b) cross-sectional view. Parameters are defined in Table 1 and in the text.

$\Delta C_{A\beta}$ and Equation 7 for λ_β/λ may be substituted into Equation 8 to give

$$J_A = S_{WSE}D_{AB}[K_1/(\lambda\lambda_\beta)] = S_{WSE}D_{AB}K_1/[(1 - K_2)(\lambda^2)]. \qquad (9)$$

Equation 9 indicates that the diffusion flux required for coarsening is inversely proportional to the square of the lamellar wavelength λ.

Because the position of a WSE changes as a result of diffusion, the migration velocity V_{WSE} of an average WSE may be obtained from Equation 9 with the help of Figure 4. The flux J_A must equal the amount of A lost in unit time from the parallelpiped of base dZ and unit height (measured perpendicular to the page in Fig. 4b). Hence,

$$J_A = (dZ/dt)(1)[(X_{A\alpha} - X_{A\beta})/v_\alpha], \qquad (10)$$

where t is the time and area dZ is defined in Figure 4b. Using Equation 10, V_{WSE} is related to J_A as follows:

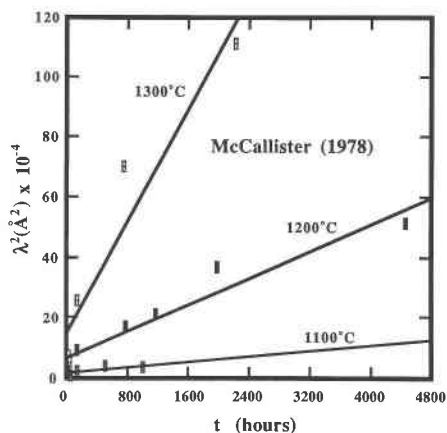$$V_{WSE} = dH/dt = (2/\lambda_\alpha)dZ/dt = 2J_Av_\alpha/[\lambda_\alpha(X_{A\alpha} - X_{A\beta})], \qquad (11)$$

Fig. 5. Coarsening data for exsolved clinopyroxenes of McCallister (1978). λ^2 is the square of the lamellar wavelength. The solid lines are least-squares fits to the expression $\lambda^2 = \lambda_0^2 + kt$ (see Table 2).

with length dH as shown in Figure 4b. Noting that $S_{WSE} = \lambda_\alpha/[2 \sin(\varphi)]$, Equations 9 and 11 combine to yield

$$V_{WSE} = K_3/(\lambda^2) \qquad (12)$$

where K_3 is a constant given by

$$K_3 = K_1 v_\alpha D_{AB}/[(1 - K_2)(X_{A\alpha} - X_{A\beta})\sin(\varphi)]. \qquad (13)$$

Equation 12 shows that the velocity of WSE migration depends on the inverse square of the lamellar wavelength λ (assuming that the shape (φ) of the WSE does not change significantly with λ). Equation 52 of Cline (1971), which gives the "velocity that the [cylindrical] plate edges recede," also shows an inverse square dependence on λ. The general form of the velocity expression (Eq. 12), like that of the driving force expression (Eq. 5), apparently does not depend on the detailed shape of the lamellar terminations.

In all of the preceding analysis, equations were developed for WSEs on α lamellae in a β host. However, the same equations may be easily modified to describe WSEs on β lamellae in the same sample (every α should be replaced by a β, every A by a B, etc.). Although the majority of WSEs occur on the lamellae of the guest phase, WSEs do occur on the host phase lamellae as well (see Fig. 2). Host WSEs will be particularly common if the volume fractions of host and guest are similar. These host WSEs can also lead to coarsening and must be considered in the overall coarsening-rate law. To see the relative importance of host WSEs, the velocity of the guest WSEs, V_{WSE}^α, can be compared with the velocity of the host WSEs, V_{WSE}^β. Assuming that the WSE angle φ and the interdiffusion coefficient D_{AB} are the same for both guest and host, Equation 12 yields

$$V_{WSE}^\alpha/V_{WSE}^\beta = (v_\alpha/v_\beta)^3(X_{A\beta}X_{B\beta}/X_{A\alpha}X_{B\alpha}). \qquad (14)$$

The cubic term in Equation 14 is likely to be near unity. If the solvus is symmetric, the composition term in Equation 14 will also be unity. Evidently, the velocities of both

host and guest lamellar WSEs will in general be similar. Therefore, in the following development, read WSE to mean *both* guest and host WSEs.

To obtain a coarsening-rate law from Equation 12, the net effect of all the WSEs must be determined. For this calculation the two-dimensional density of WSEs, i.e., the number of WSEs per unit cross-sectional area (n_{WSE}), is clearly an important parameter. For a mineral with exsolution lamellae spaced at wavelength λ, the total length of lamellae α per unit cross-sectional area is given by $1/\lambda$; the average lamellar length is $1/(\lambda n_{WSE})$. The rate of change of the total length of lamellae is given by

$$d(1/\lambda)/dt = -V_{WSE}n_{WSE}. \qquad (15)$$

WSE migration will lead to the gradual elimination of WSEs at grain boundaries or against one another. If the WSEs are randomly distributed, a change in the total length of lamellae per unit area by a certain percentage will lead to a change of the number of WSEs per unit area by the same percentage. This means that the average lamellar length $1/(\lambda n_{WSE})$ is constant and

$$\lambda n_{WSE} = \lambda_0 n_{WSE,0}, \qquad (16)$$

where the subscript 0 refers to the values of the parameters at the start of the coarsening process. Dividing Equation 15 by the (constant) average lamellar length $1/(\lambda n_{WSE})$, the rate of destruction of WSEs per unit area is found to be

$$dn_{WSE}/dt = -V_{WSE}(n_{WSE})^2 \lambda. \qquad (17)$$

The instantaneous coarsening rate follows directly from Equation 15:

$$d\lambda/dt = V_{WSE}n_{WSE}\lambda^2. \qquad (18)$$

Substituting for V_{WSE} from Equation 12 and for n_{WSE} from Equation 16, Equation 18 becomes

$$d\lambda/dt = (K_3\lambda_0 n_{WSE,0})/\lambda, \qquad (19)$$

which may be integrated to yield

$$\lambda^2 = \lambda_0^2 + kt, \qquad (20)$$

with the constant k given by

$$k = 2K_3\lambda_0 n_{WSE,0} = 2K_3\lambda n_{WSE}. \qquad (21)$$

DISCUSSION

It is common practice to fit the data of coarsening experiments with a straight line on a graph of λ vs. $t^{1/3}$. The theoretical basis for a $t^{1/3}$ rate law for coarsening was firmly established by Lifshitz and Slyozov (1961) and independently by Wagner (1961) following a preliminary study by Greenwood (1956). These authors used a statistical analysis of dispersed spherical particles to arrive at the $t^{1/3}$ result, which has stood the test of numerous experiments and theoretical refinements (e.g., Ardell, 1968, 1972; Davies et al., 1980; Tsumuraya and Miyata, 1983). Lamellar intergrowths, however, do not meet the geometric requirements of the statistical models of spheres. Further-
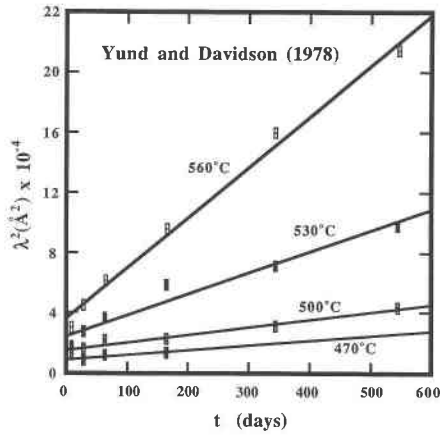
Fig. 6.   Coarsening data for exsolved clinopyroxenes of Yund and Davidson (1978). λ^2 is the square of the lamellar wavelength. The solid lines are least-squares fits to the expression $\lambda^2 = \lambda_0^2 + kt$ (see Table 2).

TABLE 2.   Reinterpreted coarsening data

T (°C)	λ_0 (m)	k (m²/s)	r	$D_{AB}\gamma_{LFS}n_{WSE,0}$ (J·m⁻²·s⁻¹)
		McCallister (1978)		
1100	1.28×10^{-8}	6.22×10^{-23}	0.810	2.75×10^{-8}
1200	2.60×10^{-8}	3.06×10^{-22}	0.964	2.81×10^{-8}
1300	3.83×10^{-8}	1.30×10^{-21}	0.961	3.42×10^{-8}
		Yund and Davidson (1978)		
470	0.94×10^{-8}	3.55×10^{-24}	0.943	
500	1.20×10^{-8}	6.01×10^{-24}	0.982	2.43×10^{-10}
530	1.56×10^{-8}	1.63×10^{-23}	0.977	2.83×10^{-10}
560	1.89×10^{-8}	3.89×10^{-23}	0.996	1.52×10^{-10}

more, the presence of lamellar terminations or "faults" mandates a different type of analysis for both lamellar and fibrous intergrowths (Graham and Kraft, 1966; Cline, 1971). As demonstrated by Equation 20, a $t^{1/3}$ rate law is not correct for the coarsening of coherent exsolution lamellae. Instead, the data of lamellar coarsening experiments should be fit with a straight line on a graph of λ^2 vs. t.

The few published experimental studies of the coarsening of mineral exsolution lamellae (Yund et al., 1974; Yund and Davidson, 1978; McCallister, 1978; Grove, 1982) have all presented data fit to the expression $\lambda = \lambda_0 + kt^{1/3}$. Although these authors recognized the lack of theoretical justification for a $t^{1/3}$ rate law for lamellar coarsening, they were unaware of Cline's (1971) work and had no other basis on which to proceed. Furthermore, in each case the data were accommodated nicely by the $t^{1/3}$ expression, although McCallister (1978) pointed out that a $t^{1/2}$ or $t^{1/4}$ expression would fit his data just as well as a $t^{1/3}$ expression. McCallister's data and Yund and Davidson's data are shown on graphs of λ^2 vs. t in Figures 5 and 6, respectively. The solid lines represent linear least-squares fits to the data points with r values, slopes, and intercepts given in Table 2. The good fit of Equation 20 to these several data sets is evidence in support of the WSE coarsening model. The intercept at $t = 0$ is taken to be λ_0, the lamellar wavelength at the start of coarsening. As might be predicted from the form of the rate laws, values of λ_0 obtained from the λ^2 rate law are higher than those obtained from the $t^{1/3}$ rate law. Interestingly, the λ_0 obtained from the λ^2 rate law are also higher than the smallest observed λ in each experiment. The values of λ_0 so calculated do increase systematically with temperature as predicted by spinodal-decomposition theory. The λ_0 values obtained by Yund and Davidson (1978) from the $t^{1/3}$ rate law do not increase systematically with temperature.

Nord (1980) and Nord and McCallister (1979) have performed further coarsening experiments with py-

roxenes. For a synthetic pyroxene of composition $Wo_{25}En_{31}Fs_{44}$, they were able to obtain a time-temperature-transformation diagram for both spinodal decomposition and coarsening in the temperature range 800 to 1050°C. In Buseck et al. (1980), Nord and McCallister found that at 1000°C, the process of spinodal decomposition takes at least 100 h. Thus, some of the data gathered by McCallister (1978) and Yund and Davidson (1978) may be documenting decomposition rather than coarsening. This might explain why the λ_0 values obtained from the λ^2 rate law are higher than some of the observed λ values.

Several interesting consequences attend the application of the WSE model to coarsening of mineral exsolution lamellae in general and to the data of McCallister (1978) and Yund and Davidson (1978) in particular. The most obvious consequence is for the extrapolation of laboratory coarsening data to geologic process. For example, Equation 20 and the data of Table 2 lead to the conclusion that the wavelength λ for coherent cryptoperthite lamellae isothermally coarsened for 10^6 yr at 500°C would be 1.38×10^5 Å. For the same isothermal coarsening, Yund and Davidson's data and the $t^{1/3}$ rate law predict that λ would be 1.10×10^4 Å, a difference of more than an order of magnitude! Fortunately, many of the published (Yund and Chapple, 1980; Grove, 1982) or imagined applications of coarsening data are for rapidly cooled rocks. The two rate laws gave comparable results for these short natural cooling experiments. A greater uncertainty is in the value of λ_0 that is produced by nonisothermal spinodal decomposition. In addition, slow cooling for long times may lead to additional coarsening processes that will dominate when coherency is lost, as is the case in some alloys (Butler and Thomas, 1970; Saunderson et al., 1978; Smartt and Courtney, 1976).

Values of the rate constant k given in Table 2 may be fit to an Arrhenius relation to determine the activation energy for coarsening. For Yund and Davidson's (1978) data, a least-squares fit of ln k vs. $1/T$ yields

$$k = (2.076 \times 10^{-14})\exp(-33.419/RT), \qquad (22)$$

where k is in m²/s and activation energy is in kcal. Yund and Davidson obtained an activation energy of 25 kcal/mol using the $t^{1/3}$ rate law. Similarly, for McCallister's (1978) data, a least-squares fit of ln k vs. $1/T$ yields

$$k = (1.472 \times 10^{-12})\exp(-65.197/RT). \quad (23)$$

Using the $t^{1/3}$ rate law, McCallister obtained an activation energy of 33 kcal/mol. Why the two rate laws should lead to such different activation energies is not entirely clear. If the rate of coarsening of the WSEs is limited by diffusion, as was assumed in deriving Equation 20, the activation energy for coarsening should be related to the activation energy for diffusion. However, because the expression for k in Equation 20 contains D_{AB}/T, the activation energy for diffusion is obtained from a least-squares fit of $\ln(kT)$ vs. $1/T$. This exercise yields activation energies for diffusion of 35 kcal/mol for the Yund and Davidson data and 68 kcal/mol for the McCallister data. Both of these numbers are low relative to the diffusion activation energies obtained from the $t^{1/3}$ rate law (75 kcal/mol for the feldspars and 99 kcal/mol for the clinopyroxenes) and low relative to activation energies obtained from other diffusion experiments (60 kcal/mol: Foland, 1974, and Kasper, 1974; and 86 kcal/mol: Brady and McCallister, 1983). However, variation with temperature of the other parameters in k, such as γ_{LFS}, λ_0, and $n_{WSE,0}$, has not been accounted for and may be responsible for this discrepancy.

Another significant consequence of the WSE model of coarsening is that the coarsening of coherent crystals exsolved by the process of spinodal decomposition depends on the two-dimensional density of WSEs ($n_{WSE,0}$) in the exsolved crystal at the start of the coarsening process. A sample with a higher $n_{WSE,0}$ would coarsen faster than a sample with a lower $n_{WSE,0}$, assuming that both had the same initial wavelength λ_0. If the value of $n_{WSE,0}$ is not the same for all exsolved crystals of the same mineral, perhaps depending on the thermal history of the crystal, then the data of coarsening experiments may not be directly applicable to all natural samples. However, if K_3 is known for the coarsening experiments, Equations 16 and 21 may be used to adjust the coarsening constant k to the $n_{WSE,0}$ of the sample in question using measured values of λn_{WSE} for the natural samples.

Unfortunately, TEM photos for the McCallister (1978) and Yund and Davidson (1978) experiments are not available. Therefore, their data cannot be applied with certainty to natural samples until K_3 (which with λ_0 gives $n_{WSE,0}$) is known or until it is demonstrated that $n_{WSE,0}$ does not vary among exsolved crystals of the same mineral. I was able to measure n_{WSE} on TEM photos of an unpublished clinopyroxene spinodal-decomposition and coarsening study by G. L. Nord, Jr., and R. H. McCallister (see p. 169–171 in Buseck et al., 1980). For samples from their 1000°C experiments (f and h in Fig. 22 of Buseck et al., 1980), n_{WSE} ranged from 1×10^{12} to 15×10^{12} m^{-2} and λn_{WSE} ranged from 1×10^5 to 5×10^5 m^{-1}. Because only a few appropriately scaled photos were available and because the WSEs are difficult to count, these numbers should be regarded as only an indication of their probable value. A statistically significant number of measurements needs to be made to verify or disprove Equation 16.

A measurement of k and several other parameters may be used with Equations 21, 13, 7, and 6 to estimate the value of the energy (γ_{LFS}) of the coherent lamellar interface. Surface energies are not well known for silicate minerals (Adamson, 1976; Brace and Walsh, 1962). Interfacial energies are even less well known, but should decrease as the misorientation between adjacent lattices decreases to zero for coherent boundaries (Kingery, 1974a, 1974b). Based on the coarsening data of McCallister (1978), the Ca-Mg interdiffusion data for pyroxenes of Brady and McCallister (1983), and a value of λn_{WSE} of 3×10^5 m^{-1} from the measurements of Nord and McCallister's photos reported above, γ_{LFS} (J/m^2) for clinopyroxenes is estimated to be 0.16 at 1100°C, 0.04 at 1200°C, and 0.011 at 1300°C. Because of large uncertainities in the diffusion data and the fact that λn_{WSE} was not measured for the samples coarsened, these interfacial energies must be considered rough estimates. Nevertheless, it is reassuring that they are in a reasonable range for surface energies and decline with rising temperature. Perhaps future coarsening experiments will provide the data required to calculate interfacial energies for exsolution lamellae with greater reliability.

REFERENCES

Adamson, A.W. (1976) Physical chemistry of surfaces, 3rd edition. Wiley, New York, 698 p.

Ardell, A.J. (1968) An application of the theory of particle coarsening: The γ' precipitate in N-Al alloys. Acta Metallurgica, 16, 511–516.

——— (1972) Isotropic fiber coarsening in unidirectionally solidified eutectic alloys. Metallurgical Transactions, 3, 1395–1401.

Brace, W.F., and Walsh, J.B. (1962) Some direct measurements of the surface energy of quartz and orthoclase. American Mineralogist, 47, 1111–1122.

Brady, J.B., and McCallister, R.H. (1983) Diffusion data for clinopyroxenes from homogenization and self-diffusion experiments. American Mineralogist, 68, 95–105.

Brady, J.B., and Stout, J.H. (1980) Normalizations of thermodynamic properties and some implications for graphical and analytical problems in petrology. American Journal of Science, 280, 173–189.

Buseck, P.R., Nord, G.L., Jr., and Veblen, D.R. (1980) Subsolidus phenomena in pyroxenes. Mineralogical Society of America Reviews in Mineralogy, 7, 117–211.

Butler, E.P., and Thomas, G. (1970) Structure and properties of spinodally decomposed Cu-Ni-Fe alloys. Acta Metallurgica, 18, 347–365.

Cline, H.E. (1971) Shape instabilities of eutectic composites at elevated temperatures. Acta Metallurgica, 19, 481–490.

Courtney, T.H. (1975) Fault migration vs. two-dimensional Ostwald ripening as a mechanism for coarsening of rod eutectics. Scripta Metallurgica, 9, 1219–1223.

Davies, C.K.L., Nash, P., and Stevens, R.N. (1980) The effect of volume fraction of precipitate on Ostwald ripening. Acta Metallurgica, 28, 179–189.

Denbigh, K. (1971) The principles of chemical equilibrium, third edition. Cambridge University Press, Cambridge, 494 p.

Foland, K.A. (1974) Alkali diffusion in orthoclase. In A.W. Hofmann, B.J. Giletti, H.S. Yoder, Jr., and R.A. Yund, Eds., Geochemical transport and kinetics, p. 77–98. Carnegie Institution of Washington and Academic Press, New York.

Fournelle, R.A. (1979a, 1979b) Discontinuous coarsening of lamellar cellular precipitate in an austentitic Fe–30 wt. %, Ni–6 wt. %, Ti alloy. I. Morphology, II. Growth kinetics. Acta Metallurgica, 27, 1135–1155.

Garmong, G., and Rhodes, C.G. (1974) The structure of interphase boundaries in Al-CuAl$_2$ curved eutectic crystals. Metallurgical Transactions, 5, 2507–2513.

Gibbs, J.W. (1906) The collected works of J. Willard Gibbs. Longmans, Green, and Company, New York, 434 p.

Graham, L.D., and Kraft, R.W. (1966) Coarsening of eutectic microstructures at elevated temperatures. Transactions of the Metallurgical Society of AIME, 236, 94–102.

Greenwood, G.W. (1956) The growth of dispersed precipitates in solutions. Acta Metallurgica, 4, 243–248.

Grove, T.L. (1982) Use of exsolution lamellae in lunar clinopyroxenes as cooling rate speedometers: An experimental calibration. American Mineralogist, 67, 251–268.

Herring, C. (1951) Surface tension as a motivation for sintering. In W.E. Kingston, Ed., The physics of powder metallurgy, p. 143–179. McGraw-Hill, New York.

Johnson, C.A. (1965) Generalization of the Gibbs-Thompson equation. Surface Science, 3, 429–444.

Kasper, R.B. (1974) Cation and oxygen diffusion in albite. Ph.D. thesis, Brown University, Providence, Rhode Island.

Kingery, W.D. (1974a) Plausible concepts necessary and sufficient for interpretation of ceramic grain-boundary phenomena: I, Grain-boundary characteristics, structure, and electrostatic potential. American Ceramic Society Journal, 57, 1–8.

——— (1974b) Plausible concepts necessary and sufficient for interpretation of ceramic grain-boundary phenomena: II, Solute segregation, grain-boundary diffusion, and general discussion. American Ceramic Society Journal, 57, 74–83.

Lewis, G.N., and Randall, M. (1961) Thermodynamics, 2nd edition, revised by K.S. Pitzer and L. Brewer. McGraw-Hill, New York, 723 p.

Lifshitz, I.M., and Slyozov, V.V. (1961) The kinetics of precipitation from supersaturated solid solutions. Journal of the Physics and Chemistry of Solids, 19, 35–50.

Lin, L.Y., and Courtney, T.H. (1974) Direct observations of lamellar fault migration in the Pb-Sn eutectic. Metallurgical Transactions, 5, 513–514.

Livingston, J.D., and Cahn, J.W. (1974) Discontinuous coarsening of aligned eutectoids. Acta Metallurgica, 22, 495–503.

McCallister, R.H. (1978) The coarsening kinetics associated with exsolution in an iron-free clinopyroxene. Contributions to Mineralogy and Petrology, 65, 327–331.

Nord, G.L., Jr. (1980) Decomposition kinetics in clinopyroxenes. Geological Society of America Abstracts with Programs, 12, 492.

Nord, G.L., Jr., and McCallister, R.H. (1979) Kinetics and mechanism of decomposition in Wo$_{25}$En$_{31}$Fs$_{44}$ clinopyroxene. Geological Society of America Abstracts with Programs, 11, 488.

Oriani, R.A. (1964) Ostwald ripening of precipitates in solid matrices. Acta Metallurgica, 12, 1399–1409.

Ostwald, W. (1900) Über die vermeintliche Isomerie des roten und gelben Quecksilberoxyds und die Oberflächenspannung fester Körper. Zeitschrift für Physikalische Chemie, 34, 495–504.

Park, M., Mitchell, T.E., and Heuer, A.H. (1976) Coarsening in a spinodally decomposing system: TiO$_2$-SnO$_2$. In H.-R. Wenk, Ed., Electron microscopy in mineralogy, p. 205–208. Springer-Verlag, New York.

Robin, P.-Y.F. (1974a) Thermodynamic equilibrium across a coherent interface in a stressed crystal. American Mineralogist, 59, 1286–1298.

——— (1974b) Stress and strain in cryptoperthite lamellae and the coherent solvus of alkali feldspars. American Mineralogist, 59, 1299–1318.

Saunderson, R.I., Wilkes, P., and Lorimer, G.W. (1978) Coarsening in the Cu-Ni-Cr system. Acta Metallurgica, 26, 1357–1370.

Smartt, H.B., and Courtney, T.H. (1976) The kinetics of coarsening in the Al-Al$_3$Ni system. Metallurgical Transactions, 7A, 123–126.

Tsumuraya, K., and Miyata, Y. (1983) Coarsening models incorporating both diffusion geometry and volume fraction of particles. Acta Metallurgica, 31, 437–452.

Wagner, C. (1961) Theorie der Alterung von Niederschlägen durch Umlösen (Ostwald-Reifung). Zeitschrift für Electrochemie, 65, 581–591.

Yund, R.A. (1984) Alkali feldspar exsolution: Kinetics and dependence on alkali interdiffusion. In W.L. Brown, Ed., Feldspar and feldspathoids: Structures, properties, and occurrences. NATO Advanced Study Institute Series C, 137, 281–315.

Yund, R.A., and Chapple, W.M. (1980) Thermal histories of two lava flows estimated from cryptoperthite lamellar spacings. American Mineralogist, 65, 438–443.

Yund, R.A., and Davidson, P. (1978) Kinetics of lamellar coarsening in cryptoperthites. American Mineralogist, 63, 470–477.

Yund, R.A., McLaren, A.C., and Hobbs, B.E. (1974) Coarsening kinetics of the exsolution microstructure in alkali feldspar. Contributions to Mineralogy and Petrology, 48, 45–55.

APPENDIX: Derivation of $\Delta C_{A\beta}$ from Equation 4

Using the standard definition (Denbigh, 1971, Equation 9.1),

$$\mu_{A\beta} = \mu_{A\beta}^0 + RT \ln(X_{A\beta}\xi_{A\beta}), \tag{A1}$$

in which $\mu_{A\beta}^0$ is the standard-state chemical potential of component A in phase β and $\xi_{A\beta}$ is an activity coefficient, Equation 4 may be rearranged as follows:

$$[\mu_{A\beta}^0 + RT \ln(X_{A\beta}^E\xi_{A\beta}^E)]X_{A\alpha}^E + [\mu_{B\beta}^0 + RT \ln(X_{B\beta}^E\xi_{B\beta}^E)]X_{B\alpha}^E$$
$$- [\mu_{A\beta}^0 + RT \ln(X_{A\beta}^\infty\xi_{A\beta}^\infty)]X_{A\alpha}^\infty - [\mu_{B\beta}^0 + RT \ln(X_{B\beta}^\infty\xi_{B\beta}^\infty)]X_{B\alpha}^\infty$$
$$= 2v_\alpha\gamma_{LFS}/\lambda_\alpha. \tag{A2}$$

The superscripts E and ∞ have been used to replace (WSE) and (∞), respectively, to shorten the notation. The standard-state chemical potentials of phase β are independent of the nature of the adjacent phase α and so need no additional superscripts. Reduction of Equation A2 to a more revealing form is not possible without some simplifying assumptions. Most helpful would be to assume that

$$X_{A\alpha}^E = X_{A\alpha}^\infty. \tag{A3}$$

This is equivalent to saying that there is no compositional variation within a lamella from its WSE to its LFS. Although this is probably not exactly correct, the difference between these two compositions will be very small indeed. Using Equation A3 then, Equation A2 becomes

$$X_{A\alpha}^\infty\ln[(X_{A\beta}^E/X_{A\beta}^\infty)(\xi_{A\beta}^E/\xi_{A\beta}^\infty)] + X_{B\alpha}^\infty\ln[(X_{B\beta}^E/X_{B\beta}^\infty)(\xi_{B\beta}^E/\xi_{B\beta}^\infty)]$$
$$= 2v_\alpha\gamma_{LFS}/(RT\lambda_\alpha). \tag{A4}$$

Another helpful assumption is that

$$(\xi_{A\beta}^{E}/\xi_{A\beta}^{\infty}) = (\xi_{B\beta}^{E}/\xi_{B\beta}^{\infty}) = 1. \tag{A5}$$

Even though the crystalline solution is significantly non-ideal in this case because the compositions are near a solvus, the compositions represented by the E and ∞ superscripts are very similar, and the respective activity coefficients will be nearly identical. Using the interfacial energies estimated above for clinopyroxenes, $(X_{A\beta}^{E} - X_{A\beta}^{\infty})$ is calculated to be on the order of 0.01. Furthermore, because the E and ∞ compositions are so similar, the approximation $\ln(x) = x - 1$ (for $x \cong 1$) may be used along with Equation A5 to reduce Equation A4 to

$$(X_{A\alpha}^{\infty}/X_{A\beta}^{\infty})(X_{A\beta}^{E} - X_{A\beta}^{\infty}) + (X_{B\alpha}^{\infty}/X_{B\beta}^{\infty})(X_{B\beta}^{E} - X_{B\beta}^{\infty})$$
$$= 2v_{\alpha}\gamma_{LFS}/(RT\lambda_{\alpha}). \tag{A6}$$

Noting that

$$(X_{A\beta}^{E} - X_{A\beta}^{\infty}) = -(X_{B\beta}^{E} - X_{B\beta}^{\infty}) \tag{A7}$$

and neglecting the difference in molar volumes between the similar compositions E and ∞, Equation A6 leads to the result

$$\Delta C_{A\beta} \equiv (X_{A\beta}^{E} - X_{A\beta}^{\infty})/v_{\beta}$$
$$= [(2v_{\alpha}\gamma_{LFS})/(RTv_{\beta}\lambda_{\alpha})][(X_{A\beta}X_{B\beta})/(X_{B\beta} - X_{B\alpha})]. \tag{A8}$$

The superscripts have been removed in Equation A8 because these are all the equilibrium (∞) values. The identity used in Equation A8, $C_{A\beta} \equiv X_{A\beta}^{E}/v_{\beta}$, is only true for "mole units" if the end-member formulas are selected properly. Equation A8 is true for any choice of end-member formulas if gram-atom units (e.g., gram-atom fraction, gram-atomic volume) are used rather than gram-formula units (see Brady and Stout, 1980). Finally, substituting the constants defined in Equations 6 and 7 of the main text, the expression given in Equation 5 is obtained:

$$\Delta C_{A\beta} = K_1/\lambda. \tag{A9}$$